Total ozone trends at three northern high-latitude stations

Leonie Bernet[1], Tove Svendby[1], Georg Hansen[1], Yvan Orsolini[1,2], Arne Dahlback[3], Florence Goutail[4], Andrea Pazmiño[4], Boyan Petkov[5,6], and Arve Kylling[1]

[1]NILU - Norwegian Institute for Air Research, Kjeller, Norway
[2]NTNU, Trondheim, Norway
[3]Department of Physics, University of Oslo, Oslo, Norway
[4]LATMOS/IPSL/USVSQ-CNRS, Guyancourt, France
[5]University G. d'Annunzio, Chieti-Pescara, Italy
[6]National Research Council, Institute of Polar Sciences (CNR-ISP), Bologna, Italy

Correspondence: Leonie Bernet (lber@nilu.no)

Abstract. After the decrease of ozone-depleting substances (ODSs) as a consequence of the Montreal Protocol, it is still challenging to detect a recovery in the total column amount of ozone (total ozone) at northern high-latitudes. To assess regional total ozone changes in the "ozone-recovery"-period (2000-2020) at northern high-latitudes, this study investigates trends from ground-based total ozone measurements at three stations in Norway (Oslo, Andøya, and Ny-Ålesund). For this purpose, we combine measurements from Brewer spectrophotometers, ground-based UV filter radiometers (GUVs), and a SAOZ instrument. The Brewer measurements have been extended to work under cloudy conditions using the global irradiance (GI) technique, which is also presented in this study. We derive trends from the combined ground-based time series with the multiple linear regression model from the Long-term Ozone Trends and Uncertainties in the Stratosphere (LOTUS) project. We evaluate various predictors in the regression model and found that tropopause pressure and lower-stratospheric temperature contribute most to ozone variability at the three stations. We report significant positive annual trends at Andøya (0.9±0.7% per decade) and Ny-Ålesund (1.5±0.1% per decade) and no significant annual trend at Oslo (0.1±0.5% per decade), but significant positive trends in autumn at all stations. Finally we found positive but insignificant trends of around 3% per decade in March at all three stations, which may be an indication for Arctic spring-time ozone recovery. Our results contribute to a better understanding of regional total ozone trends at northern high-latitudes, which is essential to assess how Arctic ozone responds to changes in ODSs and to climate change.

1 Introduction

As a consequence of the Montreal Protocol's success in reducing ozone-depleting substances (ODSs) in the stratosphere, the total column amount of ozone (total ozone) is expected to recover globally. A special focus lies on high latitudes, because they experienced the strongest stratospheric ozone depletion. Various studies showed that total ozone has started to recover in recent years in Antarctic spring (Solomon et al., 2016; Kuttippurath and Nair, 2017; Pazmiño et al., 2018; Weber et al.,

2022). In the Arctic however, a recovery is more difficult to detect. Arctic recovery may be counteracted by climate change, because cooling and moistening of the stratosphere favours the formation of polar stratospheric clouds (PSCs) which may increase seasonal ozone depletion (von der Gathen et al., 2021). Furthermore, the strong interannual and dynamical variability at northern high-latitudes makes the trend detection challenging (e.g. Langematz et al., 2018). Given these challenges, several studies investigated Arctic spring total ozone and found no significant trends (Knibbe et al., 2014; Solomon et al., 2016; Weber et al., 2018, 2022).

Most of these trend studies concentrate on the whole Arctic area and do not account for regional variability. However, Coldewey-Egbers et al. (2022) recently reported distinct regional patterns in total ozone trends based on merged satellite data, especially at northern mid- to high-latitudes (40° N to 70° N). It is therefore crucial not only to investigate trends of zonal means, but to analyse regional trends at northern high-latitudes. Whereas satellites give a global picture of ozone trends, they have the disadvantage of degradation and limited lifetimes. Ground-based instruments on the other hand provide long-term and continuous measurements and are thus ideal to investigate regional ozone trends. Only few studies have investigated regional total ozone recovery at northern high-latitudes from ground-based measurements. Global total ozone trends from ground-based and satellite data including polar regions have been extensively investigated by Weber et al. (2018, 2022), but regional trend differences were not addressed. Trends at four Arctic stations derived from ozonesonde measurements were presented by Bahramvash Shams et al. (2019), but the analysis period was short (2005 to 2017) and ozonesonde launches are generally sparse. Svendby et al. (2021) presented ground-based trends at three Norwegian stations derived with a simple linear regression, but more advanced trend analyses for Norwegian stations have only been performed for the "ozone-depletion-period" (Svendby and Dahlback, 2004; Hansen and Svenøe, 2005).

The aim of our study is to investigate regional total ozone trends from ground-based measurements at three northern high-latitude stations in Norway (Oslo, Andøya and Ny-Ålesund). For this purpose, we combine measurements from Brewer spectrophotometers, ground-based UV filter radiometers (GUVs) and a SAOZ instrument (Sect. 2). In cloudy conditions or for low solar zenith angles (SZAs), we use Brewer measurements with the Global Irradiance (GI) method (Sect. 2.1.2), which is described in detail in Appendix A. Next, we compare our combined data with satellite overpasses and ERA5 reanalyses (Sect. 3). We then derive total ozone trends by using the multiple linear regression model provided by the Long-term Ozone Trends and Uncertainties in the Stratosphere (LOTUS) project (Sect. 4). The LOTUS regression was initially developed for global ozone profile trends at low- and mid-latitudes (SPARC/IO3C/GAW, 2019). We apply it for the first time on ground-based total ozone data at high latitudes. We therefore investigate the use of various regression predictors in the LOTUS model and define a state-of-the-art set of predictors that explains the natural ozone variability at the three stations.

Finally, the remaining and unexplained ozone changes are investigated and we present annual and monthly total ozone trends for the three stations (Sect. 5).

Figure 1. Map of Europe showing the three measurement stations used in this study.

2 Total ozone data

In the present study we use total ozone data from three Brewer spectrophotometers, a SAOZ (Système d'Analyse par Observation Zénithale) instrument, and three Ground-based Ultraviolet radiometers (GUVs). Measurements are performed at the Sverdrup station at Ny-Ålesund, Svalbard (78.92° N, 11.88° E, 15 m a.s.l.), at the Arctic Lidar Observatory for Middle Atmosphere Research (ALOMAR) on Andøya (69.28° N, 16.01° E, 360 m a.s.l.), and at Oslo (Blindern and Kjeller) (Fig. 1). Measurements at Oslo have been performed in Blindern (59.95° N, 10.72° E, 96 m a.s.l.) at the University of Oslo until July 2019, afterwards the instruments were moved to the Norwegian Institute for Air Research (NILU) in Kjeller (59.98° N, 11.05° E, 139 m a.s.l.), which is located around 18 km east of Blindern. We have co-located Brewer and GUV measurements at all stations, and additional SAOZ measurements at Ny-Ålesund. All instruments provide data in the full study period (2000 to 2020), except the Brewer at Ny-Ålesund that has been operating since 2013. We use not all techniques in all months, due to limited measurement days in the winter months caused by the low sun or polar night, as indicated in Table 1. Ozone at all three stations is influenced by the polar vortex in winter and spring, with varying degrees depending on the year. Measurement availability depends on season and technique as described below.

Table 1. Data availability of all instruments used for the combined total ozone time series at the three stations.

	Oslo	Andøya	Ny-Ålesund
DS	Feb – Nov	Mar – Oct	Mar – Sept*
GI	all year	Feb – Nov	-
GUV	all year	Feb – Oct	Mar – Sept
SAOZ	-	-	Mar, Apr, Aug, Sept

*After 2013

2.1 Brewer spectrophotometers

We use ozone data from three Brewer spectrophotometers that measure UV radiation between 305 and 320 nm. The Brewer located at Oslo is a single-monochromator Brewer MKV (serial number B42), whereas a double-monochromator Brewer MKIII (B104) is located at Andøya. Both instruments are operated by NILU and have been calibrated every summer by the International Ozone Service (IOS, Canada) against a reference instrument. No calibrations were performed in 2020 and 2021 due to travel restrictions related to the COVID-19 pandemic. The Brewer at Ny-Ålesund is operated by the National Research Council, Institute of Polar Sciences (CNR-ISP), Italy. It has been calibrated by IOS in 2015 and 2018. The Brewer calibration dates are given at https://www.io3.ca/Calibrations. We investigated all calibration reports and performed some changes in the calibration files. The updates were small (mainly small calibration date corrections) and affected only a few single days. Measurements during the whole calibration period were excluded.

2.1.1 Direct sun method

For the default direct sun (DS) measurements, the Brewer instrument measures direct sunlight in the UV, as described for example in Savastiouk and McElroy (2005). Total ozone is then derived from the intensities by considering ozone absorption coefficients and Rayleigh scattering coefficients (e.g. Fioletov et al., 2011), using the O3Brewer-software (version 6.6 available at http://www.o3soft.eu/o3brewer.html). All DS measurements are regularly calibrated with daily standard lamp (SL) measurements. For the SL-correction, the intensities of an internal halogen lamp (SL) are measured at the same five wavelengths as for the ozone measurements. The SL produces a stable and continuous light spectrum. Any variations visible in the SL-measurements would also affect the ozone measurements and are therefore corrected in the routine DS calculation. The precision of DS measurements is 0.15 % (Scarnato et al., 2010) but the accuracy relies on regular calibrations (Svendby et al., 2021).

2.1.2 Global irradiance method

The Brewer DS method is limited to clear-sky conditions and solar zenith angles (SZA) below $72°$. Therefore, we use the global irradiance (GI) method to retrieve ozone from Brewer measurements in cloudy conditions and/or for larger SZA at Oslo and Andøya. In contrast to the DS method, the GI method relies on measurements of diffuse and direct irradiance, including

multiple scattering due to clouds and surface reflection. A detailed description of the method and comparison and validation of the GI data is given in Appendix A. The same method has recently been used to derive total ozone from Ground-based UV (GUV) radiometers by Svendby et al. (2021).

2.2 GUV

The ground-based UV (GUV) filter radiometers in Oslo (type GUV-511), Andøya, and Ny-Ålesund (both type GUV-541) measure direct and diffuse solar irradiance at five channels in the UV range from 305 to 380 nm. The measurements are used to derive the UV index, total ozone, biological doses, and cloud transmittance (Svendby et al., 2021). GUV ozone retrievals depend on accurate calibrations and Svendby et al. (2021) showed that the standard deviation between Brewer and GUV in Oslo and at Andøya are within 2.5% for the period 1995 to 2019. Detailed information about the GUV instruments and the measurement technique can be found in Bernhard (2005) and Svendby et al. (2021). Our GUV data corrections for seasonality and clouds are performed as described by Svendby et al. (2021).

2.3 SAOZ

The Système d'Analyse par Observation Zénithale (SAOZ) instrument at Ny-Ålesund measures solar radiation in the UV-visible range of the solar spectrum (300–650 nm). Its measurement principle and basic instrument setup is described in Pommereau and Goutail (1988). Total ozone is retrieved from the measured slant columns at sunrise and sunset, when the SZA is between 86° and 91° (Goutail et al., 2005). In order to convert measured slant columns to vertical columns, ozone air mass factor (AMF) lookup tables are used, calculated using the TOMS V8 ozone profiles (Hendrick et al., 2011). SAOZ ozone measurements present a precision of 4.7% and an accuracy of 5.9%. No measurements are available in summer when the SZA is high, and we use SAOZ data only in spring and autumn (see Table 1).

2.4 Combined ground-based total ozone data

To obtain ground-based total ozone time series with as few missing measurement days as possible, we combine total ozone measurements from the four different measurement techniques to a combined time series (GBcomb). Brewer DS and SAOZ have been used in multiple studies (e.g. Hendrick et al. (2011); Goutail et al. (2005); Scarnato et al. (2010)) and are therefore used as baseline in GBcomb. Measurements gaps are then filled with GI and GUV data. GUV data have been validated against Brewer DS and SAOZ data by Svendby et al. (2021), who found no significant biases between the datasets. GI data is evaluated in Appendix A. The Brewer DS measurements build the baseline in Oslo (53% of the measurement days) and Andøya (44%). Missing measurement days are first filled with GI data (around 40% at both stations), then with GUV (5% in Oslo and 15% in Andøya) (Fig. 2a,b). In Ny-Ålesund (Fig. 2c), we use SAOZ data as the baseline (around 35% of the measurements), and days without SAOZ measurements (mainly during summer) are filled with Brewer data (20% starting in July 2013), and with GUV data (45% after 2013). In Oslo we have data throughout the year, whereas we have measurements from February or March to October in Andøya. The combined time series at Ny-Ålesund is available from February or March to September or
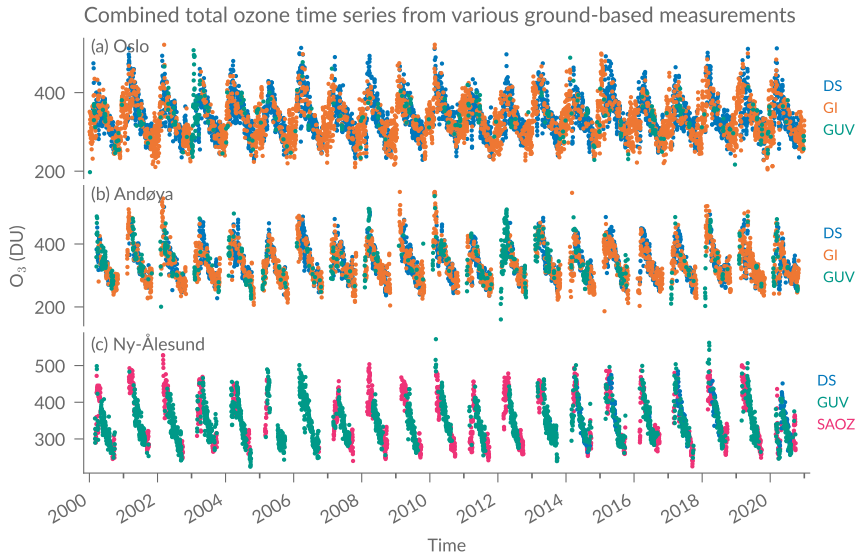
Figure 2. Daily means of total ozone from four different measurement techniques: Brewer Direct Sun (DS), Brewer Global Irradiance (GI), ground-based UV (GUV), and SAOZ, measured at **(a)** Oslo, **(b)** Andøya, and **(c)** Ny-Ålesund. DS data are the main dataset in Oslo **(a)** and Andøya **(b)**, days without DS measurements are filled with GI data, remaining missing data are then filled with GUV measurements. In Ny-Ålesund **(c)**, SAOZ is the main dataset, and DS and GUV are used to fill days with missing SAOZ data.

120   October, depending on the year. For each instrument, we compute daily means of total ozone measurements by considering measurements ± 2h around local noon. Only for SAOZ, daily means of sunset and sunrise measurements are used. Local noon is approximated by the longitude of the station, and is 11:15 UTC at Kjeller, 10:55 UTC at Andøya and 11:12 UTC at Ny-Ålesund. Outliers are excluded when the daily standard deviation exceeds ten times the mean standard deviation or if the daily mean exceeds four times the score z, where $z = (O_3 - \overline{O}_3)SD^{-1}$, with the overall mean ozone $\overline{O}_3$ and the overall standard
125   deviation SD.

2.5   Satellites

We use daily means of satellite overpass data from the Ozone Monitoring Instrument (OMI) on the Aura satellite (OMDOAO3 product) launched in 2004 and from two Global Ozone Monitoring Experiment-2 (GOME-2) instruments on the satellites Metop-A (GOME-2A, launched in 2006) and Metop-B (GOME-2B, launched in 2012). In addition we use daily overpass
130   data from the Solar Backscatter ultraviolet (SBUV) Merged Ozone Dataset (MOD) (SBUV MOD version 2 release 1), which combines total ozone measurements from several SBUV instruments (Frith et al., 2014) processed with a single retrieval algorithm (version 8.7).
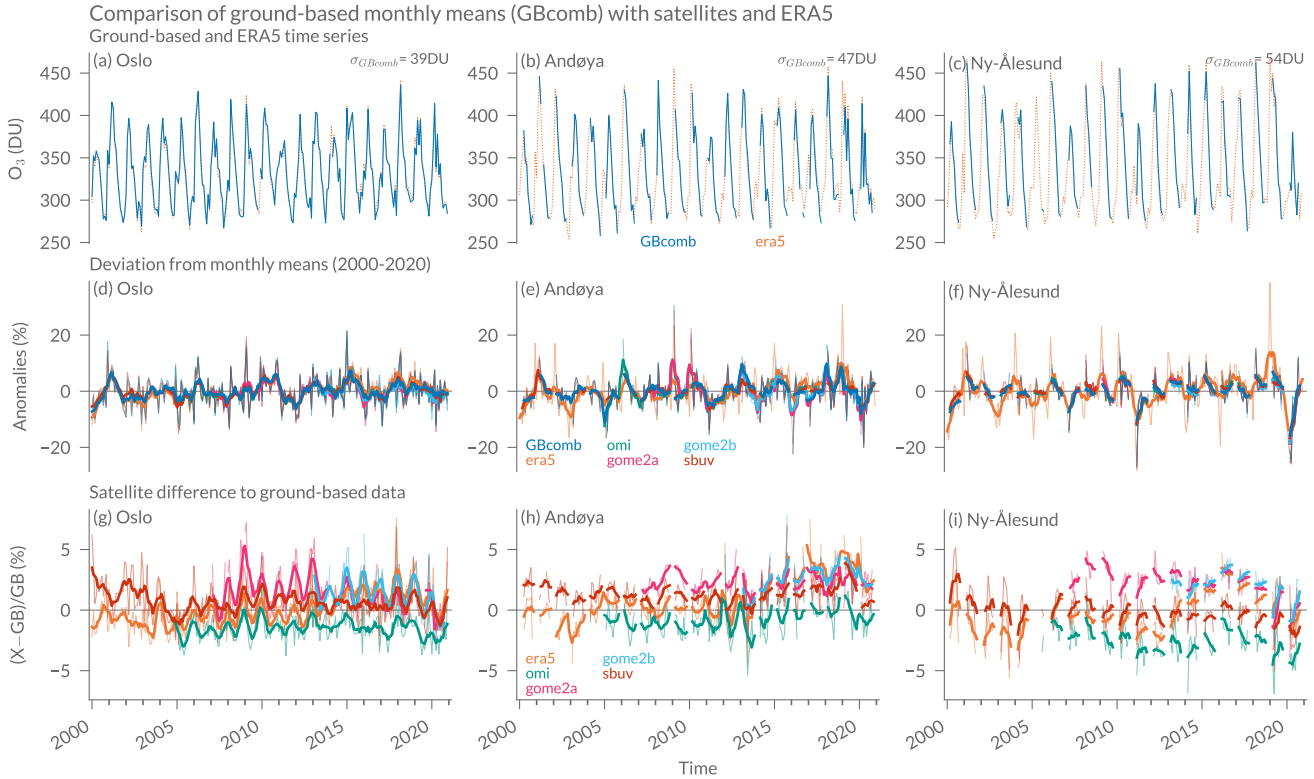
Figure 3. Comparison of the combined ground-based data (GBcomb) with satellite overpasses and ERA5 data at the three stations Oslo, Andøya and Ny-Ålesund. The first row ((**a**)–(**c**)) shows monthly means of the ground-based data together with ERA5 monthly means. The standard deviation of GBcomb data (σ_{GBcomb}) is also given. The second row ((**d**)–(**f**)) shows relative anomalies for each dataset, which are defined as the deviation of each month from the monthly mean climatology (2000–2020) of the respective dataset. The third row ((**g**)–(**i**)) shows monthly differences between GBcomb and coincident daily means of the other datasets. The thick lines in (**d**)–(**i**) show data smoothed with a moving window of 6 months (with a minimum window size of 3 months).

2.6 ERA5

We use 2-hourly data on single levels of ERA5, the atmospheric reanalysis from the European Centre for Medium Range Weather Forecasts (ECMWF) (Hersbach et al., 2018, accessed on 2021-03-24). Various total ozone satellite products are assimilated in ERA5, as described by Hersbach et al. (2020). We use ERA5 data at 10:00 and 12:00 UTC for the grid point closest to each station.

3 Time series comparison

The comparison between the combined ground-based time series (GBcomb), ERA5 reanalysis data and satellite overpasses is shown in Fig. 3. The GBcomb monthly means are shown in the first row of Fig. 3, complemented by ERA5 data to fill the seasonal measurement gaps (Fig. 3a-c). The seasonal cycle and the interannual variability is clearly visible, as well as the measurement season of the ground-based observations with missing GBcomb data in winter months at Andøya and Ny-Ålesund. The standard deviation of GBcomb data increases with latitude of the station. The second row in Fig. 3(d-f) shows the deviation from the climatology (2000-2020), the so-called anomalies. These deseasonalized monthly means show that total ozone varies naturally within around 10% at Oslo (Fig. 3d) and 20% at Andøya (Fig. 3e) and Ny-Ålesund (4f). The datasets generally agree on the natural variability and the anomalies, with larger anomalies in some years. For example, the ozone-poor year 2020 in the Arctic is clearly visible at Ny-Ålesund (Fig. 3f). Also, the strong negative anomaly in 2011 can be seen in all datasets at all stations. However, we observe that ERA5 reports more total ozone than the other datasets at all stations starting in 2014, which coincides with a change in assimilated satellite data in ERA5, as indicated by Hersbach et al. (2020) (new assimilation of METOP-B GOME-2 and change in assimilated SBUV-2 data). Furthermore, ERA5 and SBUV seem to drift from 2000 to 2005 compared to the ground-based data at all stations. Afterwards, this drift is not visible any more, suggesting that the drift may be corrected with the beginning assimiliation of Aura observations in ERA5 (Hersbach et al., 2020).

Finally, we compare differences between GBcomb, satellites and ERA5. For this, we compare daily ground-based measurements with coincident satellite overpasses and ERA5 data and show the monthly means of these differences for each station (Fig. 3(g)-(i)). On average, we observe absolute differences of 1 to 3% at all stations. This agrees with satellite uncertainties of around 2% as reported by Bodeker and Kremser (2021). We observe larger deviations for single months, but differences are never larger than 9%. In Andøya we observe a drift compared to some satellites from 2014 to 2016, which may be related to the issues with the Brewer standard lamp during this period (Sect. A4). However, we found no drift when comparing Brewer with GUV data, which makes the attribution of the origin of the drift difficult. Furthermore, we observe a similar drift when comparing ERA5 with GUV data, suggesting that ERA5 is drifting in this period of new assimilated satellite products (as mentioned above). The drift at Andøya occurs mainly compared to GOME2 and ERA5 and is less visible compared to OMI and SBUV. In Ny-Ålesund, we observe a drift in opposite direction starting in 2016. Further analyses would be required to investigate these differences. Interestingly, most satellites overestimate ozone at Ny-Ålesund in 2016 and underestimate ozone in 2020 compared to the ground-based data, which both were years with extreme cold stratospheric conditions. However, GBcomb might slightly overestimate ozone in 2020 due to high Brewer DS values after 2019. The Brewer-instrument at Ny-Ålesund was last calibrated by IOS in 2018 and a new calibration and inspection of the instrument will hopefully reveal potential problems.

4 Multiple linear regression

We use a multiple linear regression model that was developed within the activity Long-term Ozone Trends and Uncertainties in the Stratosphere (LOTUS). The so-called LOTUS regression has been tested with several ozone datasets and is described in

170 detail in SPARC/IO3C/GAW (2019). We use the model version 0.8.0 (USask ARG and LOTUS Group, 2017) and extended it by adding additional predictors (see Sect. 4.1). The following regression function is used:

$$\hat{y}(t) = a + b \cdot t + \sum_{n=1}^{4} \left(c_n \cdot \sin\left(\frac{2\pi}{l_n} \cdot t\right) + d_n \cdot \cos\left(\frac{2\pi}{l_n} \cdot t\right) \right) + \sum_{n=1}^{m} (\beta_n X_n) \tag{1}$$

with the estimated ozone time series $\hat{y}(t)$, the time vector of monthly means t, a constant intercept a and a linear term b. The seasonal cycle is considered by adding annual oscillations and some overtones (l_n = 12, 6, 4, and 3 months), with fitted
175 coefficients c_n and d_n. In addition, we include m explanatory variables X_n and their fitted coefficients β_n to explain natural variability of ozone. At Ny-Ålesund, only two seasonal components are used (l_n = 12, 6 months) due to the incomplete seasonal cycle because of missing measurements in winter. The regression coefficients are determined by minimizing a cost function, whereas uncertainties of the time series are considered in a full error covariance matrix. The model is iteratively corrected for autocorrelation according to the method by Cochrane and Orcutt (1949) (Damadeo et al. (2014, Appendix B),
180 SPARC/IO3C/GAW (2019)).

The regression is applied to monthly means from the combined daily ozone data (GBcomb). We exclude months with less than 25 measurement days to avoid values that are not representative for the whole month. This implies that at Andøya monthly means are excluded for February in several years and from November to January in all years, and at Ny-Ålesund from October to February. Monthly ozone uncertainties are considered in the error covariance matrix, using the standard error SE of each
185 monthly mean ($SE = \sigma_m n^{-\frac{1}{2}}$, with σ_m the standard deviation of the daily measurements for a particular month and n the number of measurement days for that month). We start our trend analyses in the year 2000, when a general turnaround in ODSs is assumed in polar regions (SPARC/IO3C/GAW, 2019; Weber et al., 2018; Newman et al., 2007; WMO, 2018).

4.1 Regression predictors

The aim of the regression is to assign as much ozone variability as possible to known natural variability by including various
190 predictors. By including the predictors in the regression without detrending them, any trend that is due to long-term changes in one of the predictors is removed from the ozone time series. The remaining, unexplained trend can then be attributed to changes in ODSs (Weber et al., 2022). The LOTUS regression was initially designed to derive stratospheric trend profiles for a broad set of global satellite data (SPARC/IO3C/GAW, 2019). Predictors were selected to obtain a regression that performs best in this setting. The default predictors in the LOTUS regression are: the El Niño Southern Oscillation (ENSO) (e.g. Oman et al.,
195 2013), the Quasi-Biennial Oscillation (QBO) (e.g. Baldwin et al., 2001), solar flux at 10.7cm wavelength (e.g. Lee, 2003), and aerosol optical depth (AOD, e.g. Solomon et al. (1998)). However, additional predictors may be required when using the regression for local stations, as suggested by Van Malderen et al. (2021) and SPARC/IO3C/GAW (2019). A few recent studies used the LOTUS regression to derive local trend profiles at specific stations (Godin-Beekmann et al., 2022; Bernet et al., 2021; Van Malderen et al., 2021), but they did not investigate the use of additional local predictors. Furthermore, all studies using
200 the LOTUS regression concentrate on latitudes between 60° S and 60° N and on stratospheric ozone profiles. For total ozone trends at higher latitudes, as investigated in our study, other dynamical and chemical predictors can influence ozone variability.

Table 2. Predictors investigated for use in the multiple linear regression. Predictors that have been used in the final regression are marked in bold.

Predictor	Full predictor name	Data and Source
ENSO	El Niño Southern Oscillation	Multivariate ENSO index (version 2) derived from five surface variables. https://www.esrl.noaa.gov/psd/enso/mei/data/meiv2.data
QBO(a-d)	Quasi-Biennial oscillation	Four principal components of equatorial wind at 7 pressure levels (70, 50, 40, 30, 20, 15, 10 hPa). https://www.geo.fu-berlin.de/met/ag/strat/produkte/qbo/qbo.dat
Solar	Solar flux	Adjusted solar index at 10.7 cm from OMNI. https://omniweb.gsfc.nasa.gov/form/dx1.html
AOD	Aerosol optical depth	Aerosol Extinction coefficients at 525nm from GloSSAC/NASA. Use constant after 12-2018 (last measured value). https://asdc.larc.nasa.gov/project/GloSSAC/GloSSAC_2.0
AO	Arctic oscillation	Monthly mean index from NOAA. http://www.cpc.ncep.noaa.gov/products/precip/CWlink/daily_ao_index/monthly.ao.index.b50.current.ascii
NAO	North Atlantic oscillation	Monthly mean index from NOAA. http://www.cpc.ncep.noaa.gov/products/precip/CWlink/pna/norm.nao.monthly.b5001.current.ascii
EHF	Mean Eddy heat flux	Heat flux at 100hPa from MERRA2 reanalysis, averaged over $45°$ N to $75°$ N, cumulative mean from September to April, deseasonalized. https://acd-ext.gsfc.nasa.gov/Data_services/met/ann_data.html
T50[*]	Stratospheric temperature	Deseasonalized temperature at 50hPa from ERA5 reanalysis at each station. Hersbach et al. (2019, accessed on 2021-09-03)
TropP[*]	Tropopause pressure	Deseasonalized data from NCEP reanalysis (Kalnay et al., 1996) at each station. ftp://ftp.cdc.noaa.gov/Datasets/ncep.reanalysis.derived/tropopause/pres.tropp.mon.mean.nc
TropT[*]	Tropopause temperature	Deseasonalized data from NCEP reanalysis (Kalnay et al., 1996) at each station. ftp://ftp.cdc.noaa.gov/Datasets/ncep.reanalysis.derived/tropopause/air.tropp.mon.mean.nc
VPSC	Volume of polar stratospheric clouds	Deseasonalized Polar stratospheric Cloud (PSC) NAT (nitric acid trihydrate) volume derived from MERRA2. https://ozonewatch.gsfc.nasa.gov/meteorology/temp_2020_MERRA2_NH.html

[*] Local station-specific data were used for those predictors.

A detailed overview about potential predictors that influence total ozone is given for example by Mäder et al. (2007). Various studies investigated how such predictors can be used in multiple linear regressions to derive trends at high latitudes (e.g. Knibbe et al., 2014; Kuttippurath et al., 2015; De Laat et al., 2015; Weber et al., 2022; Pazmiño et al., 2018). We investigate the use of the most relevant predictors in addition to the LOTUS default predictors. For some of them we use local data at the specific stations, and those with a strong seasonal cycle are deseasonalized, as indicated in Table 2. Our study concentrates on stratospheric ozone. The contribution of tropospheric ozone to total ozone is assumed to be small in the study time period and locations (see Sharma et al. (2013); Gaudel et al. (2018)) and tropospheric ozone variability is therefore neglected in our trend analysis.

210   For total ozone, tropopause properties are especially important, as the position of the tropopause has a strong influence on the column amount of ozone (e.g. Wohltmann et al., 2005; Varotsos et al., 2004). An increase in tropospheric height has been recently reported (Thompson et al., 2021; Meng et al., 2021), which may influence ozone trends and should thus be considered in the regression. We therefore investigate the use of station-specific tropopause pressure (TropP) and tropopause temperature (TropT) as predictors. Further, chemical ozone destruction at high latitudes is strongly linked to stratospheric temperature and

215 the occurrence of polar stratospheric clouds (PSCs). We thus inspect the use of a stratospheric temperature predictor at 50hPa (T50) and an estimator of the PSC volume (VPSC). We also examine the use of some northern teleconnection patterns, namely the Arctic oscillation (AO) and the North Atlantic oscillation (NAO). Such dynamical patterns can have an important effect on total ozone (e.g. Orsolini and Doblas-Reyes, 2003; Appenzeller et al., 2000; Brönnimann et al., 2000). The Brewer-Dobson circulation (BDC) plays an important role in explaining natural ozone variability, especially at high latitudes (e.g. Plumb,

220 2002). Its strength can be characterized by the upward propagation of planetary waves, represented by the meridional eddy heat flux (EHF) (e.g. Gabriel and Schmitz, 2003). We therefore include the mean EHF at 100hPa pressure level averaged over $45°$ N to $75°$ N as a measure of the strength of the BDC. The BDC transports ozone-rich air from the tropics towards the winter pole, and the EHF is strongest in winter. However, the transport-related variability affects not only ozone in winter and spring, but can influence the amount of ozone until the following autumn (Fioletov and Shepherd, 2003). We therefore compute a

225 cumulative mean from September to April, as suggested by Weber et al. (2018). Starting in September, each monthly EHF value is computed by averaging from September until the current month. The cumulated cold season mean (September to April) is then also used in the warm season, from May to August.

      Finally, we made some adjustments to the default use of QBO terms in the LOTUS regression. The QBO predictor is based on equatorial wind measurements at 7 pressure levels. These equatorial oscillations affect ozone beyond the tropics

230 up to polar regions (Wang et al., 2022). However, amplitude, phase and frequency of the QBO signal may change at higher latitudes (Damadeo et al., 2014). The phase- and amplitude changes can be considered by using principal components of the 7 pressure levels rather than using the direct QBO time series (Damadeo et al., 2014; SPARC/IO3C/GAW, 2019). We use the four leading principal components (QBOa-d) as suggested by Damadeo et al. (2014). Only two components were used in the LOTUS regression so far, but Anstey et al. (2021) showed that additional components are necessary to capture the recent QBO

235 disruption in northern-hemisphere winter 2019/2020. Furthermore, we added two seasonal components to the QBO predictors. This is important, because a seasonal dependence of QBO is observed at higher latitudes (Tung and Yang, 1994; Damadeo et al., 2014), which is generally not captured by regression models (Ball et al., 2019). Also, Godin-Beekmann et al. (2022) showed that the regression fit improves when seasonal components of predictors are included in the LOTUS regression.

4.2   Final choice of predictors

240 A multiple linear regression is based on the assumption that the predictors are independent. For our final selection of predictors, we therefore investigate the predictors' correlations. The Pearson correlation coefficient r for all the predictors that we investigated at Oslo are shown in Fig. 4. The significance of each coefficient has been tested with a p-value of 0.05, using a multiple test to reduce the possibility that a correlation is significant by chance (adjusted p-value). Some predictors can immediately
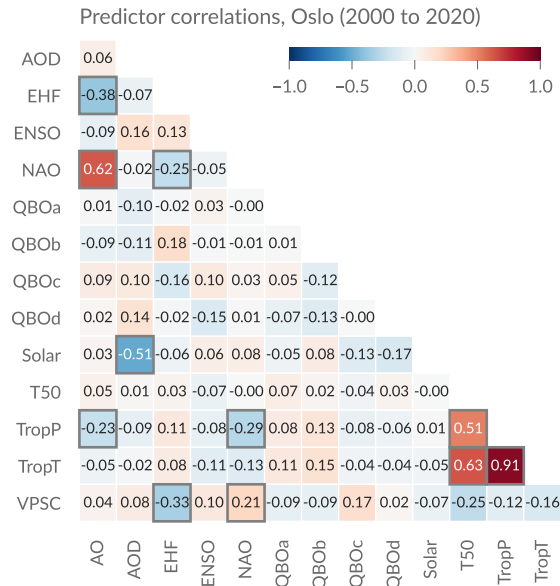
Figure 4. Pearson correlation coefficients of various predictors that are commonly used to account for natural ozone variability. The predictors that are location-specific are shown for Oslo (TropP, TropT and T50), the other predictors are station-independent. Significant correlations are marked with a grey border. The significance has been tested with a p-value of 0.05 using a multiple test to reduce the possibility that a correlation is significant by chance (adjusted p-value).

be excluded because of their high correlation to another predictor. For example, tropopause pressure (TropP) and tropopause

245 temperature (TropT) should not be used both because they are significantly correlated ($r = 0.91$). We decide to use TropP and not TropT, because the tropopause altitude has a large influence on total ozone (e.g. Steinbrecht et al., 1998; Varotsos et al., 2004). Furthermore, the circulation patterns NAO and AO are significantly correlated ($r = 0.62$) and should not be used both in the regression. TropP and T50 are also significantly correlated ($r = 0.51$), but their simultaneous use is further discussed below. Finally, there is a significant correlation between AOD and the solar flux ($r = -0.51$). This might be a spurious correlation in

250 the selected time period, where AOD was generally low because no major volcanic eruption occurred. Indeed, no correlation between solar flux and AOD is observed for a longer time period from 1979 to 2020 (not shown). The ozone effect from AOD is mainly relevant for important volcanic eruptions (e.g. Solomon et al., 1998) and we therefore decide not to use AOD in our regression.

Besides the independence and the physical meaningfulness of the predictors, it is important to study the improvement of the

255 regression fit when a specific predictor is included. Based on these aspects, we decided on a final set of predictors used in the regression fit. First, we decided to use T50, even though it is correlated to TropP, because including T50 substantially improves the adjusted coefficient of determination (R^2_{adj}) of the annual model fit (e.g. from 0.91 to 0.96 at Oslo) and for most months. To be sure that the correlation between both does not affect the interpretation of our results, we also inspected the fit for a
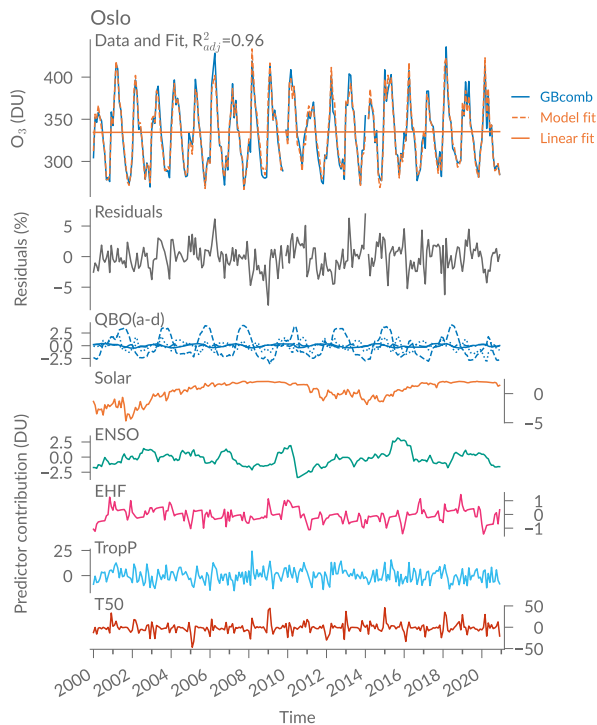
Figure 5. Regression fit, residuals and predictor contribution ($\beta_n \cdot X_n$, with coefficient β_n and predictor X_n) at Oslo.

possible multicollinearity by investigating the variance inflation factor (VIF). We used a VIF threshold of 5, which means that
260   no collinearity problem is assumed when testing the regression with each predictor as dependent variable as long as VIF<5
(e.g. Schuenemeyer and Drew, 2010). We observed multicollinearity only for monthly trends at Oslo in March ($\text{VIF}_{\text{TropP}} = 5.2$)
and September ($\text{VIF}_{\text{T50}} = 5.5$) and at Ny-Ålesund in September ($\text{VIF}_{\text{TropP}} = 5.0$), but not for annual trends.

Second, we decided not to include the dynamical predictors NAO and AO, because they are weakly but significantly corre-
lated with TropP and EHF (Fig. 4). These large-scale predictors should be well represented in the local predictors (TropP), as
265   also suggested by Mäder et al. (2007). Also, there is no important improvement in the model performance when NAO and AO
predictors are included. Finally, we do not include VPSC because of the weak but significant correlation to EHF (Fig. 4) and
no general improvement in R^2_{adj}, even though we observe that the fit at Ny-Ålesund is improved (smaller residuals) in some
extreme years when VPSC is included (not shown). The temperature-dependent chemical activity is already covered by using
T50, which in addition represents circulation changes in the stratosphere. The chosen predictors that are finally used in the
270   regression are marked in bold in Table 2.

Figure 5 shows the contribution of the selected predictors to the regression fit at Oslo using the full time series, further
referred to as annual trend fit. The model is well representing the data with a R^2_{adj} of 0.96, which indicates that the regression
fit can explain 96% of the ozone variation at Oslo. The residuals generally lie within 5% and a spectral analysis of the residuals
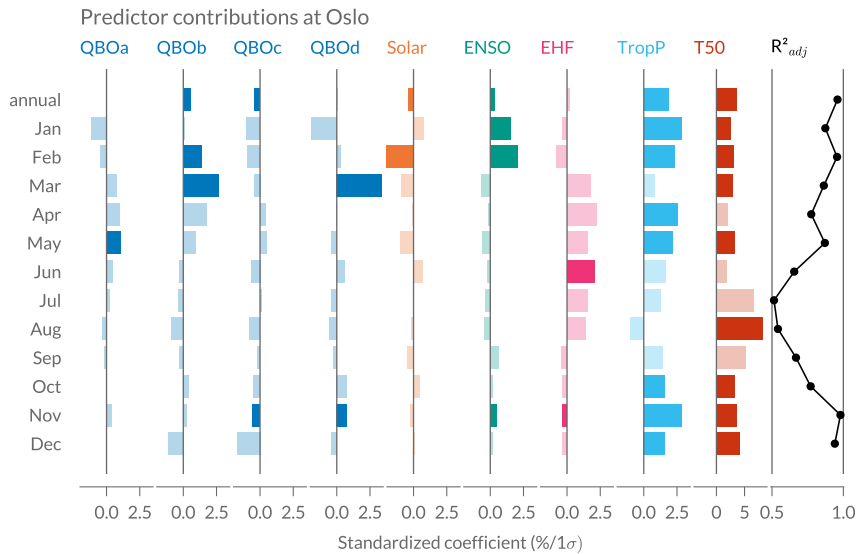
13

Figure 6. Predictor contribution to the regression fit at Oslo for the annual regression fit and individual monthly fits. The standardized coefficients describe the percentage change in ozone for a 1-standard-deviation change in the predictor. Pale color bars indicate that the predictor's contribution to ozone is not significant (p-value of the coefficient <0.05). The last panel on the right shows the adjusted coefficient of determination (R^2_{adj}) for the annual and all monthly fits. Note that the range of the x-axis is different for T50 than for the other predictors.

(not shown) suggests that the dominant patterns that influence ozone variation are captured by the regression. The lower panels in Fig. 5 show that most of the ozone variation can be explained by T50 and TropP (predictors with largest contribution), followed by two of the QBO-terms (QBOb and QBOc). The solar flux, ENSO and EHF have only small contributions to ozone variability at Oslo. However, all predictors have a significant contribution to the regression fit except the EHF and 3 of the QBO components (see annual trend in Fig.6). At Andøya and Ny-Ålesund, the EHF contribution to the annual fit is significant, but some of the default predictor coefficients (Solar, ENSO and QBO) become insignificant (see Figs. B1 and B2). This confirms results by Bahramvash Shams et al. (2019) based on ozonesonde measurements in the Arctic and by Vigouroux et al. (2015) based on FTIR measurements.

The predictor coefficients, their significance, and the model's performance for individual monthly fits at Oslo are shown in Fig.6. The coefficients have been standardized to make a direct comparison possible. The standardized coefficients β_{std} describe the percentage change in ozone for a 1-standard-deviation change in the predictor, according to Brunner et al. (2006):

$$\beta_{std} = \beta \frac{\sigma_X}{\bar{y}} \cdot 100 \tag{2}$$

with the predictor coefficient β, the standard deviation σ_X of predictor X and the mean ozone value $\bar{y}$. Generally, the largest contribution to total ozone is provided by the T50 predictor, followed by TropP (Fig. 6). Whereas most predictors contribute significantly to the annual regression fit and to most monthly fits in winter, the regression coefficients are mostly insignificant in the summer months (pale shading in Fig. 6). This poor explanation of ozone variability in summer by the predictors is

reflected in lower values of R^2_{adj} from June to September (R^2_{adj} between 0.5 and 0.7), with particular low values in July and August (0.51 and 0.54). In most other months, however, the ozone variation at Oslo is well captured by the model, with R^2_{adj} ranging from 0.77 (October) to 0.98 (November). Total ozone in summer is generally driven by photochemistry and less by the transport-related predictors, which may explain the poorer model performance in summer. Furthermore, the interannual variability is generally low in summer and may be dominated by natural variability or noise, as suggested by Brunner et al. (2006).

In Ny-Ålesund and Andøya, we observe high R^2_{adj} in March and September and smaller values in the other months, especially in April (both stations) and May (only at Ny-Ålesund) (see Figs. B1 and B2). However, the R^2_{adj} at those stations is generally lower than in Oslo, especially at Ny-Ålesund. This can be explained by the high interannual variability at Andøya and Ny-Ålesund (compare Fig. 3) that makes it more difficult to explain the ozone variability with the predictors used.

5   Trend results

5.1   Annual trends

Annual trend fits (using the full time series) and their residuals for the three stations are shown in Fig. 7 and represented in Table 3. At all stations, we observe that the model represents the data well, with R^2_{adj} values of 0.96 (Oslo and Andøya) and 0.97 (Ny-Ålesund). The residuals lie within 5%, with some outliers of up to 10% in Andøya and Ny-Ålesund, where the model captures less well the ozone variability (e.g. in 2008 or 2020). The standard errors of the residuals (SE_{res}) of 1.53 DU (Oslo) to 2.63 DU (Ny-Ålesund) indicate that the predicted values differ from the true ozone values by less than 1% on average. We observe significant positive total ozone trends at Andøya and Ny-Ålesund of 0.9±0.7 and 1.5±1.0% per decade respectively, and a trend of almost zero (0.1±0.5% per decade) at Oslo (see Fig. 7 and Table 3). Trends are expressed as percentage of the mean ozone value at each station and a trend is declared to be significantly different from zero at a 95 % confidence interval as soon as its absolute value exceeds twice its uncertainty (e.g. Tiao et al., 1990).

Positive trends of similar magnitudes have also been found for Scandinavia or the North Atlantic in previous satellite-based studies. For example, Sofieva et al. (2021) found positive trends over Scandinavia of 1 to 5 % per decade depending on altitude based on merged satellite ozone profile data from 2003 to 2018 (their Fig. 10), and Coldewey-Egbers et al. (2022) reported significant positive total ozone trends of 1.2% per decade in the North Atlantic sector based on merged total ozone data from 1997 to 2020 (their Table 3 and Fig. 3). Furthermore, Svendby et al. (2021) analysed total ozone trends with a simple linear regression from 1999 to 2019, using ground-based GUV measurements at the same three stations as in our study. They found similar trend magnitudes, but slightly larger uncertainties (1.5±1.8% per decade at Oslo, 0.5±2.6% per decade at Andøya, 1.2±2.4% per decade at Ny-Ålesund). In contrast to our results at Andøya and Ny-Ålesund, their annual trends were not significant, which suggests that the use of multiple predictors in our study can successfully reduce trend uncertainties at the two northernmost stations.
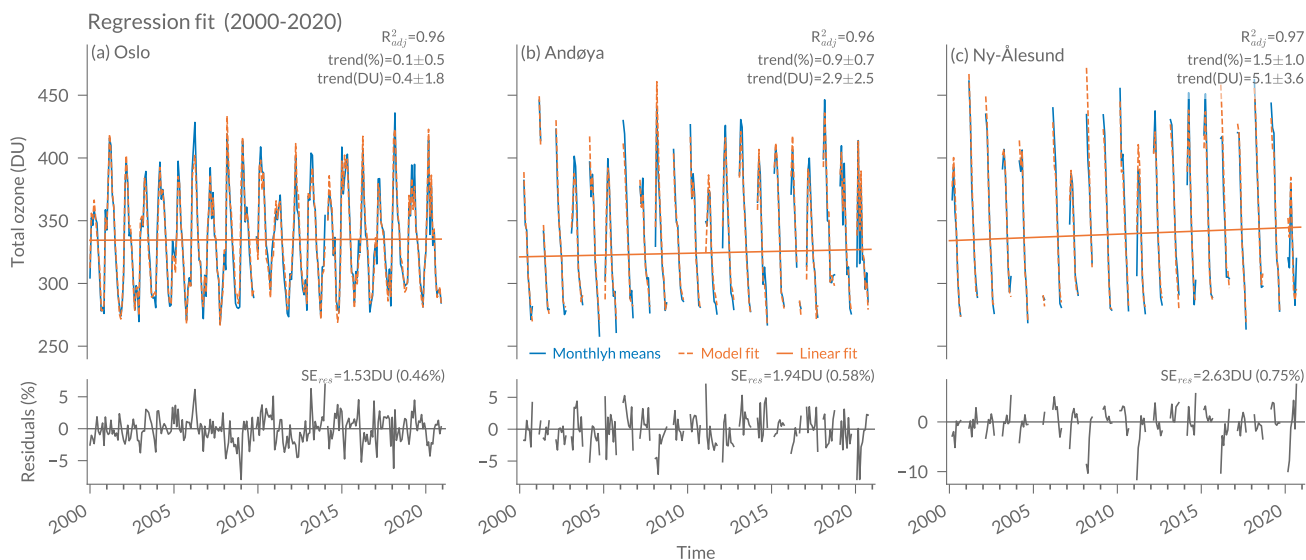
15

Figure 7. Regression fit of total ozone for **(a)** Oslo, **(b)** Andøya, and **(c)** Ny-Ålesund. The resulting linear trend is given in % per decade and DU per decade with 2-standard-deviation (σ) uncertainties. The lower panels show the residuals of the regression fit in percent ((Data–Model)/Data) and the standard error of the residuals (SE_{res}) in DU and percent (compared to the mean ozone value at each station).

Table 3. Trend values for annual regression fits of total ozone (2000 to 2020) with R^2_{adj} and the standard errors of the residuals (SE_{res}). Trends that are significantly different from zero at 95% confidence interval are marked in bold. The second column shows monthly trends that are significantly different from zero.

Station	Latitutde	Longitude	Trend (%/dec.)	Trend (DU/dec.)	R^2_{adj}	SE_{res}(%)	Significant monthly trends (%/dec.)
Oslo	59.95° N	10.72° E	0.1±0.5	0.4±1.8	0.96	0.46	Feb (**-4.3±2.2**)
							Oct (**2.4±1.5**)
							Nov (**1.4±0.7**)
Andøya	69.28° N	16.01° E	**0.9±0.7**	**2.9±2.5**	0.96	0.58	Aug (**2.5±2.0**)
Ny-Ålesund	78.92° N .	11.88° E	**1.5±1.0**	**5.1±3.6**	0.97	0.75	Sept (**3.5±2.8**)

5.2 Monthly trends

Monthly trends were computed for all stations by applying the regression to the time series of each month, usually including 21 data points for each month (2000 to 2020). We do not include February trends at Andøya because the time series is short (only 15 years) due to sparse February measurements in some years. The monthly trends are illustrated in Figure 8 and significant trends are given in Table 3.

325

16

Trends in late spring and summer months (May to July) are not significantly different from zero at 95% confidence interval at all stations and almost zero at Oslo. However, in late summer and autumn (August to November), we observe significant positive ozone trends at Oslo (October: 2.4±1.5% and November: 1.4±0.7% per decade), Andøya (August: 2.5±2.0%) and Ny-Ålesund (September: 3.5±2.8% per decade). Our significant autumn trends confirm results by Svendby et al. (2021), who found significant trends at Oslo of 3.23±2.01% in fall from 1999 to 2019 using a simple linear regression. In contrast to our results, Morgenstern et al. (2021) found significant negative trends in September and October at 80° N, using satellite zonal means. These contrasting results suggest that it is important to investigate regional trends and not only zonal means.

In Winter (December to February), we only derive trends in Oslo due to the missing data (polar night) at the other stations. Winter Oslo trends are positive but insignificant in December and January, and significantly negative in February (-4.3±2.2% per decade). The negative February trend in Oslo persists even if we exclude the extreme year 2020 from the regression. This negative trend may be specific for the selected time period: in the first five years (2000-2005) we have rather stable February monthly means, afterwards we observe more interannual variability and several years with specially low ozone, which results in a negative trend. Furthermore, we observe a significant negative contribution of the solar predictor to February ozone at Oslo as visible in Fig. 6. Longer time series and additional stations would need to be investigated to analyse this effect further. Interestingly, the Oslo February fit is remarkably good compared to other months, with a R^2_{adj} of 0.96 (see Fig. 6), indicating that the predictors used can well capture the high year-to-year variability in February.

Ozone trends in spring months are of special interest in polar regions, because those regions experienced strongest ozone depletion in the pre-2000 phase (e.g. Solomon, 1999). At the two northernmost stations (Ny-Ålesund and Andøya), our analyses report positive but insignificant ozone trends in March and April. The trend uncertainties are high, related to the large interannual variability. In April, the model fit is less good than in most other months, with R^2_{adj} of 0.33 (Ny-Ålesund) and 0.49 (Andøya), indicating that April ozone variability is less well explained by the predictors used in our regression. In March, however, R^2_{adj} values are at least 0.86 at all three stations. The March time series and the corresponding regression fits are shown in Fig. 9. Even though the March trends are not significantly different from zero (at 95% confidence) due to large trend uncertainties, it is remarkable that all three station data agree on similar positive ozone trends of around 3% per decade and that the regression model can reproduce the ozone variability so well.

Positive but insignificant March trends in the Arctic (60° N to 90° N) have also been reported by Weber et al. (2018) based on zonal satellite and ground-based data, who found trends of 1.2±3.7% per decade (with 2-σ uncertainties) from 2000 to 2016 and slightly larger trends when extending to 2020 (2.0±3.9%, Weber et al. (2022)). Our March trends at the three stations are slightly larger than those zonal mean trends. These results confirm previous studies reporting zonally asymmetric trends with larger trends over the Atlantic and Scandinavian sector compared to other longitudes at northern high-latitudes (Zhang et al., 2019; Sofieva et al., 2021; Coldewey-Egbers et al., 2022).
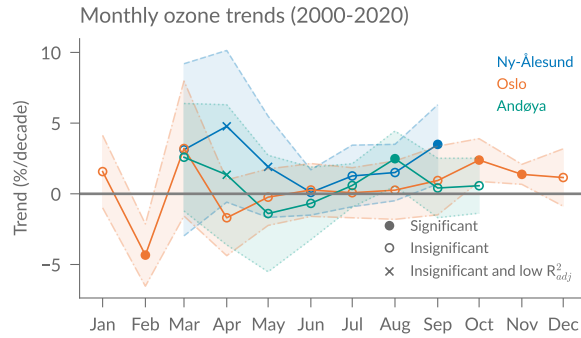
Figure 8. Monthly ozone trends in percent per decade for the three stations, with 2-σ uncertainty shadings. Filled dots represent trends that are significantly different from zero at the 95% confidence interval. Fits with low $R^2_{adj} < 0.5$ are marked with crosses.
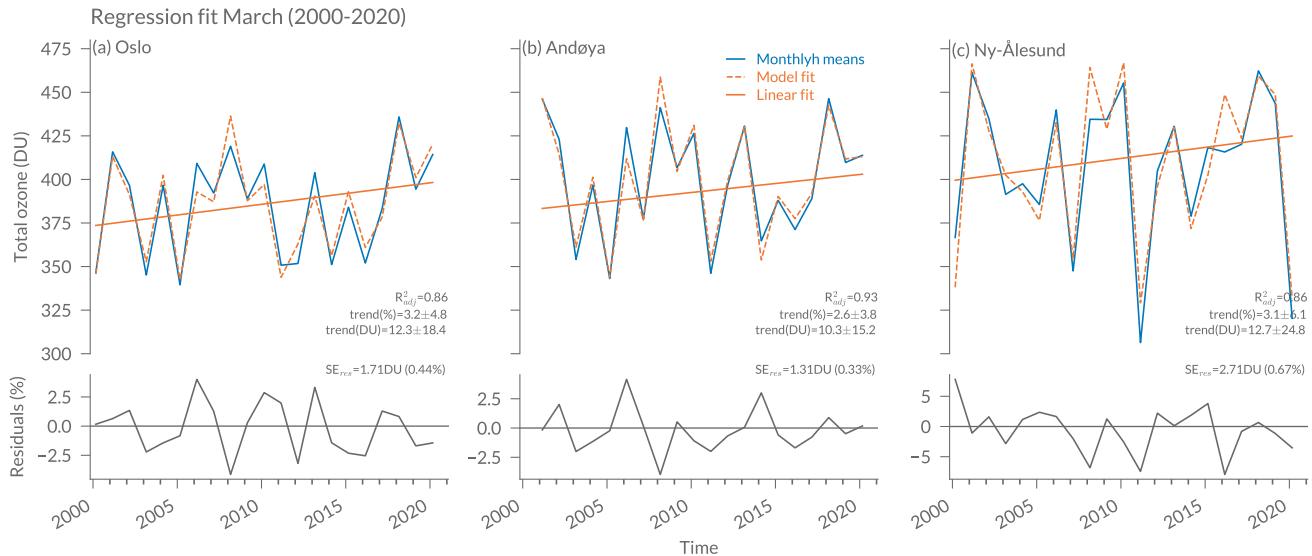

Figure 9. Same as Fig. 7 but for the month of March.

6 Conclusions

This study investigates ground-based total ozone trends at the northern high-latitude stations Oslo, Andøya and Ny-Ålesund. We presented combined total ozone time series at the three stations with measurements from four measurement techniques (Brewer DS, Brewer GI, SAOZ, and GUV). The combination of various techniques makes it possible to overcome measurement gaps due to instrumental limitations. The combined time series were compared with satellite overpass data and ERA5 reanalysis. All datasets agree on average within 1 to 3 % with the ground-based time series.

To derive total ozone trends from 2000 to 2020, we used the LOTUS regression model for the first time for ground-based total ozone data at high latitudes. Additional regression predictors have been examined and a set of predictors has been identified that should be considered when deriving total ozone trends at northern high-latitudes. We examined various predictors that are commonly used to account for natural ozone variability by checking their correlations and contributions to the regression fit. We found that tropopause pressure and lower-stratospheric temperature are dominant predictors that contribute significantly to ozone in most months. Our results further show that the trend model with the selected predictors represents well the total ozone variability at the selected stations, with high coefficients of determination (R^2_{adj} >0.95). We found significant trends of 0.9 % per decade at Andøya and 1.5% per decade at Ny-Ålesund, but no significant trends at Oslo when looking at the full time series (annual trends). Our monthly regression analyses indicate significant positive trends in autumn at Oslo (October and November) and late summer at the northernmost stations Andøya and Ny-Ålesund (August or September). Finally, we observe positive trends of around 3% per decade in Arctic spring (March) but the trends are not significantly different from zero. Nevertheless, these springtime trends and the significant autumn trends might be an indication for Arctic ozone recovery due to changes in ODSs.

In conclusion, our study emphasizes the need to concentrate on regional ozone trends rather than zonal means when investigating Arctic ozone recovery. Long-term ground-based measurements of total ozone can contribute to this aim by verifying satellite-derived trends on a regional scale. Our results contribute to a better understanding of regional total ozone trends at northern high-latitudes, which is essential to assess how Arctic ozone responds to changes in ODSs and to climate change.

Code and data availability. The combined time series used in this study – including daily SAOZ means and noon measurements of Brewer DS, Brewer GI, and GUV – are provided at https://doi.org/10.5281/zenodo.6760259 (Bernet et al., 2022). The full Brewer GI data can be found at https://doi.org/10.5281/zenodo.6760244 (Svendby et al., 2022). The full time series of Brewer DS daily means are available at the World Ozone and Ultraviolet Radiation Data Centre (https://woudc.org). SAOZ data are available at http://www.ndacc.org/. GUV data (v2.0) are available at https://doi.org/10.5281/zenodo.4773478 (Svendby, 2021), and are used here with some updates (extended to 2020, and calibrated in 2019 and 2020). OMI and GOME-2 overpass data are available at the Aura validation centre, for OMI (OMDOAO3) through https://avdc.gsfc.nasa.gov/pub/data/satellite/Aura/OMI/V03/L2OVP/OMDOAO3 (Veefkind, 2006, accessed 30.11.2021) and for GOME-2A and GOME-2B through https://avdc.gsfc.nasa.gov/pub/data/satellite/MetOp/GOME2/V03/L2OVP/. The SBUV MOD data are available at https://acd-ext.gsfc.nasa.gov/Data_services/merged/. The NCEP Reanalysis Derived data used for tropopause predictors were provided by the NOAA/OAR/ESRL PSL, Boulder, Colorado, USA, from their website at https://psl.noaa.gov/data/gridded/data.ncep.reanalysis.derived.tropopause.html. The other sources for the predictors used in the trend model are given in Table 2. The python version of the GI processing programme is available upon request (tms@nilu.no).

Appendix A: Global irradiance (GI) method

A1   GI retrieval

The most accurate estimates of total ozone amount in the atmosphere with the Brewer spectrophotometer use direct sun (DS)
measurements. The DS procedure is based on simultaneous measurements of direct solar radiation I_i at four UV wavelengths (i
= 2,3,4,5) with different ozone absorption coefficients. The wavelenghts used are 310.1 nm, 313.5 nm, 316.8 nm, and 320.1 nm
all with a 0.6 nm bandwidth (full width at half maximum, FWHM) (SCI-TEC Instruments, 1999). Combining the radiation at
the four wavelengths we obtain:

$$N(x,\theta_s) = \frac{I_4(x,\theta_s)}{I_2(x,\theta_s)} \cdot \left(\frac{I_4(x,\theta_s)}{I_3(x,\theta_s)}\right)^{-0.5} \cdot \left(\frac{I_5(x,\theta_s)}{I_4(x,\theta_s)}\right)^{-1.7} \tag{A1}$$

where x is the ozone amount and θ_s is the solar zenith angle (SZA). The values -0.5 and -1.7 are weights that minimize effects
of SO_2 absorption on $N(x,\theta_s)$. Radiances of direct sunlight passing through the atmosphere are attenuated according to Beer's
law. As the ozone absorption coefficients and molecular scattering cross-sections for the different wavelengths used are known,
the total ozone amount x can be found by taking the logarithm of N and considering the known absorption coefficients, the air
mass factor and the background intensity (see e.g. Savastiouk and McElroy (2005), WMO (2008, Chapter 16), Fioletov et al.
(2011)).

When clouds obscure the sun, the radiances I do not obey Beer's law because diffuse (scattered) radiation becomes important. Therefore, the simple logarithm procedure fails. In the GI (global irradiance) method, the radiances I in Eq. A1 are
replaced by irradiances E, i.e. the sum of the direct and diffuse radiation falling on a flat horizontal surface. The global irradiances are measured through the UV dome of the Brewer instead of the flat quarts window used for DS measurements. The
modified radiation for GI, $N_{GI}(x,\theta_s)$, is:

$$N_{GI}(x,\theta_s) = \frac{E_4(x,\theta_s)}{E_2(x,\theta_s)} \cdot \left(\frac{E_4(x,\theta_s)}{E_3(x,\theta_s)}\right)^{-0.5} \cdot \left(\frac{E_5(x,\theta_s)}{E_4(x,\theta_s)}\right)^{-1.7} \tag{A2}$$

The $N_{GI}(X,\theta_s)$ is simulated with a multiple scattering pseudo-spherical radiative transfer model (Stamnes et al., 1988;
Dahlback and Stamnes, 1991) for various x and θ_s to obtain a lookup table. Light scattering on air molecules depends strongly
on wavelength (Rayleigh scattering). In clouds, the wavelength dependency is considerably smaller due to the much larger
sizes of cloud particles compared to air molecules (Mie scattering). Since the N_{GI}-values are based on irradiance ratios, the
sensitivity to clouds is expected to be small, at least for thin clouds. Thus the lookup table is calculated for clear sky and a
surface albedo of 5% pertinent for snow- and ice-free surfaces. The sensitivity of ozone profiles to the irradiances (and hence
the N_{GI}-values) increases with θ_s. Therefore, a profile climatology for low, middle, or high latitudes (McPeters et al., 1998)
can be chosen to compute the N_{GI}-value lookup tables. The ozone amount x is then determined by finding the N_{GI}-value in
the lookup table that agrees with the observed N_{GI}.

A2 GI calibration

The radiation detector in the Brewer is a photomultiplier tube (PMT). The irradiance for a particular wavelength is proportional to its count rate C_i ($i = 2,3,4,5$). The N_{GI}-value can be written as

$$N_{GI}(x,\theta_s) = r \cdot \frac{C_4(x,\theta_s)}{C_2(x,\theta_s)} \cdot \left(\frac{C_4(x,\theta_s)}{C_3(x,\theta_s)}\right)^{-0.5} \cdot \left(\frac{C_5(x,\theta_s)}{C_4(x,\theta_s)}\right)^{-1.7} \tag{A3}$$

425 where r is a calibration factor that is determined by utilizing a reliable ozone DS measurement with the Brewer. By choosing a day with clear sky, preferably around noon, the r value is determined such that Eq. A3 agrees with the N_{GI}-value in the lookup table for the observed DS ozone value and SZA θ_s. We performed a GI calibration as soon as we observed severe changes in the Brewer standard lamp (SL). In Andøya, we calibrated GI in 06-2001, 08-2014, 08-2016, 08-2018, and 08-2019, for Oslo we used new calibration files in 08-2005 and twice in summer 2019 (see Fig. A2).

430 The Oslo Brewer is equipped with a single monochromator. It is well known that stray light in the single Brewer optics causes errors in measured ozone at large θ_s and particularly for large ozone amounts. Therefore, for low sun ($\theta_s > 72°$) we replace the four-wavelength ratios in Eqs. A2 and A3 by a single ratio of 316.8 nm to 313.5 nm. The motivation for this is that we avoid 310.1 nm-radiation that is the wavelength that is mostly affected by stray light in Eq. A2.

In order to filter out cases where thick clouds are difficult to correct, we define a cloud transmission factor CLT:

435 $$CLT = cr \cdot \frac{C_{5,meas}(x,\theta_s)}{E_{5,clearsky}(x,\theta_s)} \tag{A4}$$

$C_{5,meas}$ is the measured irradiance (count rate), $E_{5,clearsky}$ is the clear-sky irradiance calculated with the radiative transfer model for a snow- and ice-free surface. The factor cr is a calibration factor that is determined by using measurements on a day with cloud-free and snow-free conditions with CLT = 1 (100%).

A3 GI processing

440 The GI method described above will normally work well without further corrections. However, to optimize the measurements, we have taken instrumental drift (SL changes) into account, as described in Sect. 2.1.1. for DS measurements. Further, we performed minor cloud- and SZA corrections, based on the comparison to DS measurements. Similar corrections have been used by Svendby et al. (2021) on measurements from ground-based UV (GUV) radiometers. The SZA correction is mainly relevant for the winter season when the combination of a changed atmospheric profile and low sun can introduce errors to the

445 ozone value retrieved from the lookup table. To obtain corrected GI values (GI$_{corr}$), we derive a correction function $f(i)$ from the linear relationship between the DS/GI-ratio and the solar angle ($i =$SZA) as well as DS/GI and the cloud transmittance ($i =$CLT):

$$\text{GI}_{corr}(t) = \text{GI}(t) \cdot f(i) \tag{A5}$$

with

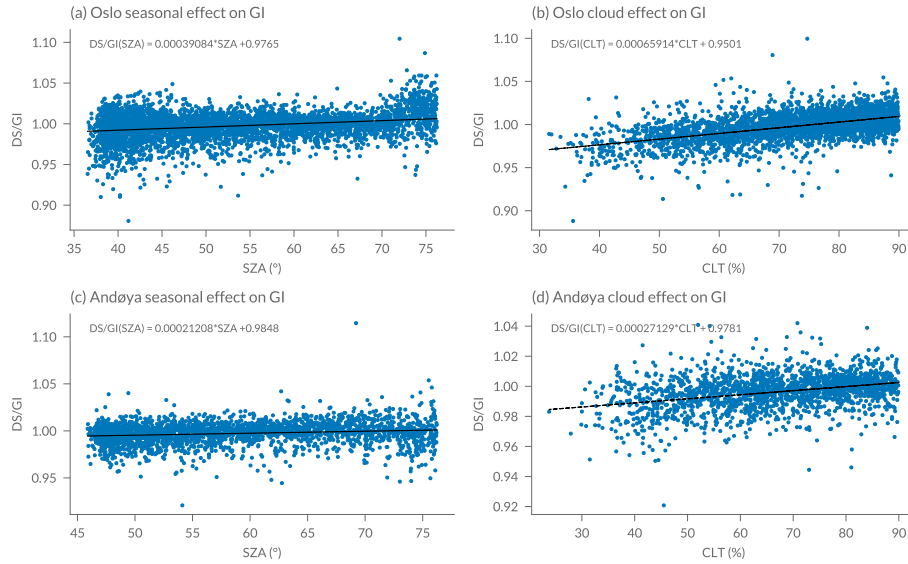450 $$f(i) = \frac{\text{DS}(i)}{\text{GI}(i)} = a_i \cdot i + b_i. \tag{A6}$$

Figure A1. Linear relationships between the DS/GI-ratio and **(a,c)** the solar angle (SZA) as well as **(b,d)** the cloud transmittance (CLT) for Oslo (1995 to 2020) and Andøya (2000 to 2020).

Table A1. Linear fit between DS/GI-ratio and solar zenith angle (SZA) and cloud transmittance (CLT) used for the GI correction in Eq. A6.

Station	a_{SZA}	b_{SZA}	a_{CLT}	b_{CLT}
Oslo	3.9084×10^{-4}	0.9765	6.5914×10^{-4}	0.9501
Andøya	2.1208×10^{-4}	0.9848	2.7129×10^{-4}	0.9781

The correction coefficients are derived by comparing GI to DS measurements from 1995 to 2020 in Oslo and from 2000 to 2020 in Andøya, as shown in Fig. A1. The derived coefficients are given in Table A1. The CLT correction is only applied for cloudy situations (CLT< 90%). Finally, we excluded GI data for situations with low cloud transmittance (CLT< 20%) and situations with $\theta_s > 84°$.

455 **A4 GI validation**

Fig. A2 shows the comparison of GI daily means with coincident DS data at Oslo and Andøya. On average, we observe an absolute difference between GI and DS of around 1% at both stations, indicating a good agreement. We observe a slightly higher difference before 2005 at Oslo and after 2015 at Andøya. These episodes coincide with rapid changes in the SL values.

To validate the GI measurements with independent data, we compared GI daily means also with coincident reanalysis data
460 (ERA5) at both stations (Fig. A3). In addition, we show Brewer data from the Zenith Sky (ZS) method that is commonly used to retrieve ozone in cloudy conditions (e.g. Fioletov et al., 2011). We observe a good agreement with ERA5 data, with an
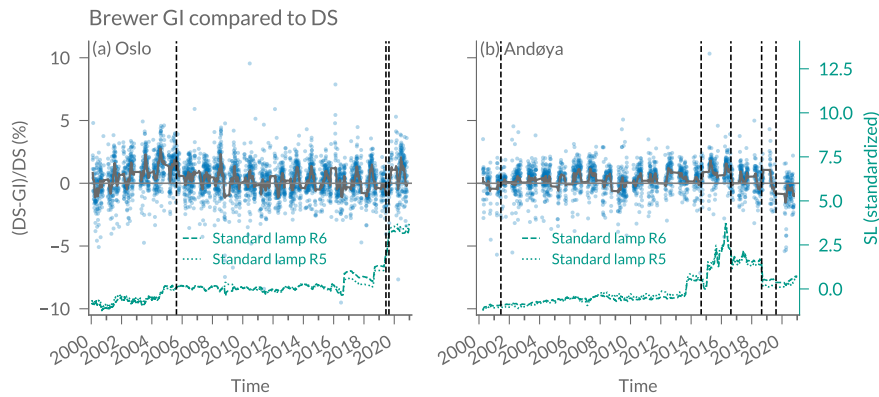
Figure A2. Brewer Global Irradiance (GI) data compared to DS data at **(a)** Oslo and **(b)** Andøya. Data smoothed with a moving mean window of 30 days is shown by the thick grey lines. The right axis shows standard lamp (SL) ratios R5 and R6, standardized to zero mean and standard deviation of one, smoothed with a mowing mean window of 30 days. Vertical dashed lines show dates that were used for GI calibration.

average absolute difference between ERA5 and GI of 2.3±2.5% at Andøya and 2.2±2.1% at Oslo. We further observe that GI measurements agree slightly better with ERA5 than ZS measurements, especially at Andøya (3.3% difference between ZS and ERA5). Fig. A2 also shows the SL measurements for the two SL ratios R5 and R6 and shows large changes in the standard

465 lamp in Andøya between 2015 and 2018. Such irregularities can partly be handled thanks to the regular calibrations and the SL correction in the GI retrieval (see Appendix A2), but we observe larger differences to ERA5 in this period (Fig. A3). However, similar anomalies are observed when comparing ERA5 to GUV data at Andøya, suggesting that ERA5 is also showing a drift from 2015 onwards.

Our results show that the GI method can provide ozone data of higher quality than the commonly used ZS method. The

470 advantage of GI is that it can also be used at high SZA, and the measurement season at high latitudes can therefore be extended in winter months when the sun is low. Furthermore, the GI method is based on physical measurements, whereas the ZS method is normally based on purely statistically derived relationships.
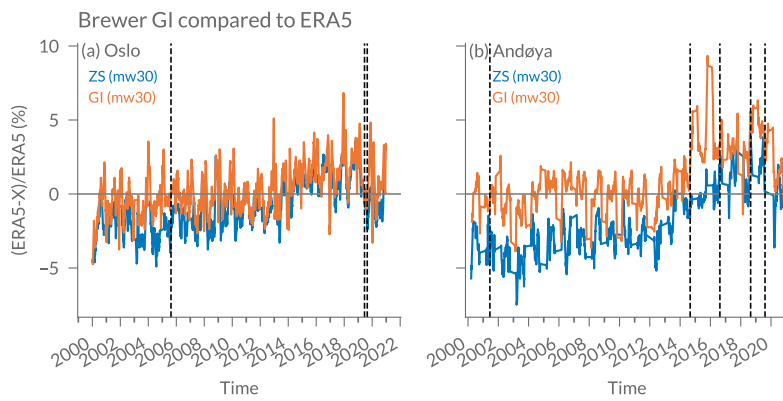
Figure A3. Brewer Global Irradiance (GI) data and Brewer Zenith sky (ZS) data, both compared to ERA5 data at **(a)** Oslo and **(b)** Andøya. The time series have been smoothed with a moving mean window of 30 days. Vertical dashed lines show dates that were used for GI calibration.
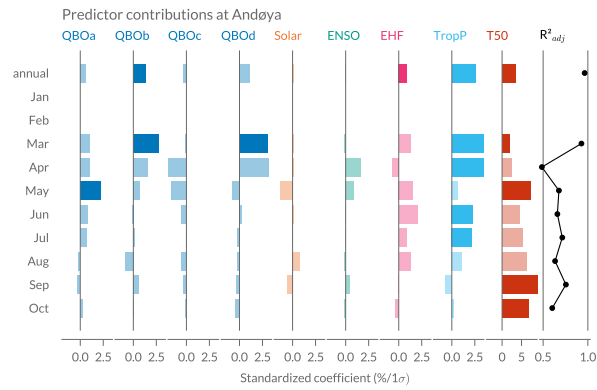
Figure B1. Predictor contribution to the regression fit at Andøya for the annual regression fit and individual monthly fits. The last panel on the right shows the adjusted coefficient of determination (R^2_{adj}) for the annual and all monthly fits. Note that the range of the x-axis is different for T50 than for the other predictors.
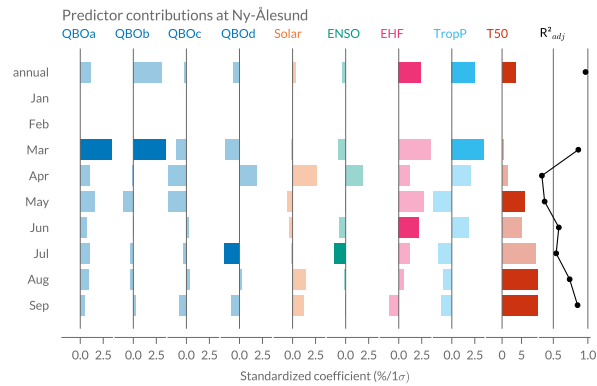
Figure B2. Same as Fig. B1 but for Ny-Ålesund.

Appendix B: Regression predictors at additional stations

Similar as Fig. 5 for Oslo, the following figures show the monthly contributions of predictors used in the regression model for Andøya (Fig. B1) and Ny-Ålesund (Fig. B2).

References

Anstey, J. A., Banyard, T. P., Butchart, N., Coy, L., Newman, P. A., Osprey, S., and Wright, C.: Prospect of increased disruption to the QBO in a changing climate, Earth Space Sci. Open Arch., pp. 1–24, https://doi.org/10.1002/essoar.10503358.3, 2021.

Appenzeller, C., Weiss, A. K., and Staehelin, J.: North Atlantic Oscillation modulates total ozone winter trends, Geophys. Res. Lett., 27, 1131–1134, https://doi.org/10.1029/1999GL010854, 2000.

Bahramvash Shams, S., Walden, V. P., Petropavlovskikh, I., Tarasick, D., Kivi, R., Oltmans, S., Johnson, B., Cullis, P., Sterling, C. W., Thölix, L., Errera, Q., Bahramvash Shams, S., Walden, V. P., Petropavlovskikh, I., Tarasick, D., Kivi, R., Oltmans, S., Johnson, B., Cullis, P., Sterling, C. W., Thölix, L., and Errera, Q.: Variations in the vertical profile of ozone at four high-latitude Arctic sites from 2005 to 2017, Atmospheric Chem. Phys., 19, 9733–9751, https://doi.org/10.5194/acp-19-9733-2019, 2019.

Baldwin, M. P., Gray, L. J., Dunkerton, T. J., Hamilton, K., Haynes, P. H., Randel, W. J., Holton, J. R., Alexander, M. J., Hirota, I., Horinouchi, T., Jones, D. B. A., Kinnersley, J. S., Marquardt, C., Sato, K., and Takahashi, M.: The Quasi-Biennial Oscillation, Rev. Geophys., 39, 179–229, https://doi.org/http://dx.doi.org/10.1029/1999RG000073; doi:10.1029/1999RG000073, 2001.

Ball, W. T., Alsing, J., Staehelin, J., Davis, S. M., Froidevaux, L., and Peter, T.: Stratospheric ozone trends for 1985-2018: Sensitivity to recent large variability, Atmospheric Chem. Phys., 19, 12 731–12 748, https://doi.org/10.5194/acp-19-12731-2019, 2019.

Bernet, L., Boyd, I., Nedoluha, G., Querel, R., Swart, D., and Hocke, K.: Validation and trend analysis of stratospheric ozone data from ground-based observations at Lauder, New Zealand, Remote Sens., 13, 1–15, https://doi.org/10.3390/rs13010109, 2021.

Bernet, L., Svendby, T., Hansen, G., Goutail, F., Pazmiño, A., and Petkov, B.: Combined ground-based total ozone data at three Norwegian sites (2000 to 2020) (version v1.0), https://doi.org/10.5281/zenodo.6760259, 2022.

Bernhard, G.: Real-time ultraviolet and column ozone from multichannel ultraviolet radiometers deployed in the National Science Foundation's ultraviolet monitoring network, Opt. Eng., 44, 041 011, https://doi.org/10.1117/1.1887195, 2005.

Bodeker, G. E. and Kremser, S.: Indicators of Antarctic ozone depletion: 1979 to 2019, Atmospheric Chem. Phys., 21, 5289–5300, https://doi.org/10.5194/acp-21-5289-2021, 2021.

Brönnimann, S., Luterbacher, J., Schmutz, C., Wanner, H., and Staehelin, J.: Variability of total ozone at Arosa, Switzerland, since 1931 related to atmospheric circulation indices, Geophys. Res. Lett., 27, 2213–2216, https://doi.org/10.1029/1999GL011057, 2000.

Brunner, D., Staehelin, J., Maeder, J. A., Wohltmann, I., and Bodeker, G. E.: Variability and trends in total and vertically resolved stratospheric ozone based on the CATO ozone data set, Atmospheric Chem. Phys., 6, 4985–5008, https://doi.org/10.5194/acp-6-4985-2006, 2006.

Cochrane, D. and Orcutt, G. H.: Application of Least Squares Regression to Relationships Containing Auto-Correlated Error Terms, J. Am. Stat. Assoc., 44, 32–61, https://doi.org/10.1080/01621459.1949.10483290, 1949.

Coldewey-Egbers, M., Loyola, D. G., Lerot, C., and Van Roozendael, M.: Global, regional and seasonal analysis of total ozone trends derived from the 1995–2020 GTO-ECV climate data record, Atmospheric Chem. Phys., 22, 6861–6878, https://doi.org/10.5194/acp-22-6861-2022, 2022.

Dahlback, A. and Stamnes, K.: A new spherical model for computing the radiation field available for photolysis and heating at twilight, Planetary and Space Science, 39, 671–683, https://doi.org/10.1016/0032-0633(91)90061-E, 1991.

Damadeo, R. P., Zawodny, J. M., and Thomason, L. W.: Reevaluation of stratospheric ozone trends from SAGE II data using a simultaneous temporal and spatial analysis, Atmospheric Chem. Phys., 14, 13 455–13 470, https://doi.org/10.5194/acp-14-13455-2014, 2014.

De Laat, A. T., Van Der A, R. J., and Van Weele, M.: Tracing the second stage of ozone recovery in the Antarctic ozone-hole with a "big data" approach to multivariate regressions, Atmospheric Chem. Phys., 15, 79–97, https://doi.org/10.5194/acp-15-79-2015, 2015.

Fioletov, V. E. and Shepherd, T. G.: Seasonal persistence of midlatitude total ozone anomalies, Geophys. Res. Lett., 30, https://doi.org/10.1029/2002GL016739, 2003.

Fioletov, V. E., McLinden, C. A., McElroy, C. T., and Savastiouk, V.: New method for deriving total ozone from Brewer zenith sky observations, J. Geophys. Res. Atmospheres, 116, 1–10, https://doi.org/10.1029/2010JD015399, 2011.

525 Frith, S. M., Kramarova, N. A., Stolarski, R. S., McPeters, R. D., Bhartia, P. K., and Labow, G. J.: Recent changes in total column ozone based on the SBUV Version 8.6 Merged Ozone Data Set, J. Geophys. Res. Atmospheres, 119, 9735–9751, https://doi.org/10.1002/2014JD021889, 2014.

Gabriel, A. and Schmitz, G.: The Influence of Large-Scale Eddy Flux Variability on the Zonal Mean Ozone Distribution, J. Climate, 16, 2615–2627, https://doi.org/10.1175/1520-0442(2003)016<2615:TIOLEF>2.0.CO;2, 2003.

530 Gaudel, A., Cooper, O. R., Ancellet, G., Barret, B., Boynard, A., Burrows, J. P., Clerbaux, C., Coheur, P. F., Cuesta, J., Cuevas, E., Doniki, S., Dufour, G., Ebojie, F., Foret, G., Garcia, O., Granados-Muñoz, M. J., Hannigan, J. W., Hase, F., Hassler, B., Huang, G., Hurtmans, D., Jaffe, D., Jones, N., Kalabokas, P., Kerridge, B., Kulawik, S., Latter, B., Leblanc, T., Le Flochmoën, E., Lin, W., Liu, J., Liu, X., Mahieu, E., McClure-Begley, A., Neu, J. L., Osman, M., Palm, M., Petetin, H., Petropavlovskikh, I., Querel, R., Rahpoe, N., Rozanov, A., Schultz, M. G., Schwab, J., Siddans, R., Smale, D., Steinbacher, M., Tanimoto, H., Tarasick, D. W., Thouret, V., Thompson, A. M., 535 Trickl, T., Weatherhead, E., Wespes, C., Worden, H. M., Vigouroux, C., Xu, X., Zeng, G., and Ziemke, J.: Tropospheric Ozone Assessment Report: Present-day distribution and trends of tropospheric ozone relevant to climate and global atmospheric chemistry model evaluation, Elementa, 6, https://doi.org/10.1525/elementa.291, 2018.

Godin-Beekmann, S., Azouz, N., Sofieva, V., Hubert, D., Petropavlovskikh, I., Effertz, P., Ancellet, G., Degenstein, D. A., Zawada, D., Froidevaux, L., Wild, J., Davis, S., Steinbrecht, W., Leblanc, T., and Querel, R.: Updated trends of the stratospheric ozone vertical distri540 bution in the 60 ° S-60 ° N latitude range based on the LOTUS regression model, Atmospheric Chem. Phys. Discuss., pp. 1–28, 2022.

Goutail, F., Pommereau, J. P., Lefèvre, F., Van Roozendael, M., Andersen, S. B., Kåstad Høiskar, B. A., Dorokhov, V., Kyrö, E., Chipperfield, M. P., and Feng, W.: Early unusual ozone loss during the Arctic winter 2002/2003 compared to other winters, Atmospheric Chem. Phys., 5, 665–677, https://doi.org/10.5194/acp-5-665-2005, 2005.

Hansen, G. and Svenøe, T.: Multilinear regression analysis of the 65-year Tromsø total ozone series, J. Geophys. Res. Atmospheres, 110, 545 1–11, https://doi.org/10.1029/2004JD005387, 2005.

Hendrick, F., Pommereau, J. P., Goutail, F., Evans, R. D., Ionov, D., Pazmino, A., Kyró, E., Held, G., Eriksen, P., Dorokhov, V., Gil, M., and Van Roozendael, M.: NDACC/SAOZ UV-visible total ozone measurements: Improved retrieval and comparison with correlative ground-based and satellite observations, Atmospheric Chem. Phys., 11, 5975–5995, https://doi.org/10.5194/acp-11-5975-2011, 2011.

Hersbach, H., Bell, B., Berrisford, P., Biavati, G., Horányi, A., Muñoz Sabater, J., Nicolas, J., Peubey, C., Radu, R., Rozum, I., Schepers, D., 550 Simmons, A., Soci, C., Dee, D., and Thépaut, J.-N.: ERA5 hourly data on single levels from 1979 to present, Copernicus Climate Change Service (C3S) Climate Data Store (CDS), https://doi.org/10.24381/cds.adbb2d47, 2018.

Hersbach, H., Bell, B., Berrisford, P., Biavati, G., Horányi, A., Muñoz Sabater, J., Nicolas, J., Peubey, C., Radu, R., Rozum, I., Schepers, D., Simmons, A., Soci, C., Dee, D., and Thépaut, J.-N.: ERA5 monthly averaged data on pressure levels from 1979 to present, Copernicus Climate Change Service (C3S) Climate Data Store (CDS), https://doi.org/10.24381/cds.6860a573, 2019.

555 Hersbach, H., Bell, B., Berrisford, P., Hirahara, S., Horányi, A., Muñoz-Sabater, J., Nicolas, J., Peubey, C., Radu, R., Schepers, D., Simmons, A., Soci, C., Abdalla, S., Abellan, X., Balsamo, G., Bechtold, P., Biavati, G., Bidlot, J., Bonavita, M., Chiara, G., Dahlgren, P., Dee, D., Diamantakis, M., Dragani, R., Flemming, J., Forbes, R., Fuentes, M., Geer, A., Haimberger, L., Healy, S., Hogan, R. J., Hólm, E.,

28

Janisková, M., Keeley, S., Laloyaux, P., Lopez, P., Lupu, C., Radnoti, G., Rosnay, P., Rozum, I., Vamborg, F., Villaume, S., and Thépaut, J.-N.: The ERA5 global reanalysis, Q. J. R. Meteorol. Soc., 146, 1999–2049, https://doi.org/10.1002/qj.3803, 2020.

560 Kalnay, E., Kanamitsu, M., Kistler, R., Collins, W., Deaven, D., Gandin, L., Iredell, M., Saha, S., White, G., Woollen, J., Zhu, Y., Leetmaa, A., Reynolds, R., Chelliah, M., Ebisuzaki, W., Higgins, W., Janowiak, J., Mo, K. C., Ropelewski, C., Wang, J., Jenne, R., and Joseph, D.: The NCEP/NCAR 40-Year Reanalysis Project, Bull. Am. Meteorol. Soc., 77, 437–471, https://doi.org/10.1175/1520-0477(1996)077<0437:TNYRP>2.0.CO;2, 1996.

Knibbe, J. S., Van Der A, R. J., and De Laat, A. T.: Spatial regression analysis on 32 years of total column ozone data, Atmospheric Chem.
565 Phys., 14, 8461–8482, https://doi.org/10.5194/acp-14-8461-2014, 2014.

Kuttippurath, J. and Nair, P. J.: The signs of Antarctic ozone hole recovery, Sci. Rep., 7, https://doi.org/10.1038/s41598-017-00722-7, 2017.

Kuttippurath, J., Godin-Beekmann, S., Lefèvre, F., Santee, M. L., Froidevaux, L., and Hauchecorne, A.: Variability in Antarctic ozone loss in the last decade (2004-2013): High-resolution simulations compared to Aura MLS observations, Atmospheric Chem. Phys., 15, 10 385–10 397, https://doi.org/10.5194/acp-15-10385-2015, 2015.

570 Langematz, U., Tully, M., Calvo, N., Dameris, M., Laat, J., Klekociuk, A., Müller, R., and Young, P.: Polar stratospheric ozone: Past, present, and future, Chapter 4 in WMO scientific Assessment of Ozone Depletion: 2018, in: Scientific Assessment of Ozone Depletion: 2018, Global Ozone Research and Monitoring Project – Report No. 58, vol. 58, World Meteorological Organization, Geneva, Switzerland, 2018.

Lee, H.: Simulation of the combined effects of solar cycle, quasi-biennial oscillation, and volcanic forcing on stratospheric ozone changes in recent decades, J. Geophys. Res., 108, 4049, https://doi.org/10.1029/2001JD001503, 2003.

575 Mäder, J. A., Staehelin, J., Brunner, D., Stahel, W. A., Wohltmann, I., and Peter, T.: Statistical modeling of total ozone: Selection of appropriate explanatory variables, J. Geophys. Res. Atmospheres, 112, 1–16, https://doi.org/10.1029/2006JD007694, 2007.

McPeters, R. D., Bhartia, P. K., Krueger, A. J., Herman, J. R., Wellemeyer, C. G., Seftor, C. J., Jaross, G., Torres, O., Moy, L., Labow, G., Byerly, W., Taylor, S. L., Swissler, T., and Cebula, R. P.: Earth Probe Total Ozone Mapping Spectrometer (TOMS) Data Products User's Guide, Tech. Rep. 1998-206895, National Aeronautics and Space Administration, Goddard Space Flight Center, Lanham, Maryland, USA,
580 1998.

Meng, L., Liu, J., Tarasick, D. W., Randel, W. J., Steiner, A. K., Wilhelmsen, H., Wang, L., and Haimberger, L.: Continuous rise of the tropopause in the Northern Hemisphere over 1980–2020, Sci. Adv., 7, eabi8065, https://doi.org/10.1126/sciadv.abi8065, 2021.

Morgenstern, O., Frith, S. M., Bodeker, G. E., Fioletov, V., and van der A, R. J.: Reevaluation of Total-Column Ozone Trends and of the Effective Radiative Forcing of Ozone-Depleting Substances, Geophys. Res. Lett., 48, e2021GL095 376,
585 https://doi.org/10.1029/2021GL095376, 2021.

Newman, P. A., Daniel, J. S., Waugh, D. W., and Nash, E. R.: A new formulation of equivalent effective stratospheric chlorine (EESC), Atmospheric Chem. Phys., 7, 4537–4552, https://doi.org/10.5194/acp-7-4537-2007, 2007.

Oman, L. D., Douglass, A. R., Ziemke, J. R., Rodriguez, J. M., Waugh, D. W., and Nielsen, J. E.: The ozone response to ENSO in Aura satellite measurements and a chemistry-climate simulation: OZONE RESPONSE TO ENSO, J. Geophys. Res. Atmos., 118, 965–976,
590 https://doi.org/10.1029/2012JD018546, 2013.

Orsolini, Y. J. and Doblas-Reyes, F. J.: Ozone signatures of climate patterns over the Euro-Atlantic sector in the spring, Q. J. R. Meteorol. Soc., 129, 3251–3263, https://doi.org/10.1256/qj.02.165, 2003.

Pazmiño, A., Godin-Beekmann, S., Hauchecorne, A., Claud, C., Khaykin, S., Goutail, F., Wolfram, E., Salvador, J., and Quel, E.: Multiple symptoms of total ozone recovery inside the Antarctic vortex during austral spring, Atmospheric Chem. Phys., 18, 7557–7572,
595 https://doi.org/10.5194/acp-18-7557-2018, 2018.

Plumb, R. A.: Stratospheric transport, J. Meteorol. Soc. Jpn., 80, 793–809, https://doi.org/10.2151/jmsj.80.793, 2002.

Pommereau, J. P. and Goutail, F.: O3 and NO2 ground-based measurements by visible spectrometry during Arctic winter and spring 1988, Geophys. Res. Lett., 15, 891–894, https://doi.org/10.1029/GL015i008p00891, 1988.

Savastiouk, V. and McElroy, C. T.: Brewer spectrophotometer total ozone measurements made during the 1998 Middle Atmosphere Nitrogen Trend Assessment (MANTRA) Campaign, Atmosphere - Ocean, 43, 315–324, https://doi.org/10.3137/ao.430403, 2005.

Scarnato, B., Staehelin, J., Stübi, R., and Schill, H.: Long-term total ozone observations at Arosa (Switzerland) with Dobson and Brewer instruments (1988–2007), J. Geophys. Res. Atmospheres, 115, https://doi.org/10.1029/2009JD011908, 2010.

Schuenemeyer, J. H. and Drew, L. J.: Regression, in: Statistics for Earth and Environmental Scientists, pp. 99–149, John Wiley & Sons, Ltd, Hoboken, New Jersey, https://doi.org/10.1002/9780470650707.ch4, 2010.

SCI-TEC Instruments: BREWER MKIV Spectrophotometer Operator's Manual, Tech. Rep. OM-BA-C231 REV B, SCI-TEC Instruments Inc., Saskatoon, Sask., Canada, 1999.

Sharma, S., Ishizawa, M., Chan, D., Lavoué, D., Andrews, E., Eleftheriadis, K., and Maksyutov, S.: 16-year simulation of Arctic black carbon: Transport, source contribution, and sensitivity analysis on deposition, J. Geophys. Res. Atmospheres, 118, 943–964, https://doi.org/10.1029/2012JD017774, 2013.

Sofieva, V. F., Szelag, M., Tamminen, J., Kyrölä, E., Degenstein, D., Roth, C., Zawada, D., Rozanov, A., Arosio, C., Burrows, J. P., Weber, M., Laeng, A., Stiller, G. P., Von Clarmann, T., Froidevaux, L., Livesey, N., Van Roozendael, M., and Retscher, C.: Measurement report: Regional trends of stratospheric ozone evaluated using the MErged GRIdded Dataset of Ozone Profiles (MEGRIDOP), Atmospheric Chem. Phys., 21, 6707–6720, https://doi.org/10.5194/acp-21-6707-2021, 2021.

Solomon, S.: Stratospheric ozone depletion: A review of concepts and history, Rev. Geophys., 37, 275–316, https://doi.org/10.1029/1999RG900008, 1999.

Solomon, S., Portmann, R. W., Garcia, R. R., Randel, W., Wu, F., Nagatani, R., Gleason, J., Thomason, L., Poole, L. R., and McCormick, M. P.: Ozone depletion at mid-latitudes: Coupling of volcanic aerosols and temperature variability to anthropogenic chlorine, Geophys. Res. Lett., 25, 1871–1874, https://doi.org/10.1029/98GL01293, 1998.

Solomon, S., Ivy, D. J., Kinnison, D., Mills, M. J., Neely, R. R., and Schmidt, A.: Emergence of healing in the Antarctic ozone layer, Science, 353, 269–274, https://doi.org/10.1126/science.aae0061, 2016.

SPARC/IO3C/GAW: SPARC/IO3C/GAW Report on Long-term Ozone Trends and Uncertainties in the Stratosphere, SPARC Report No. 9, GAW Report No. 241, WCRP-17/2018, https://doi.org/10.17874/f899e57a20b, 2019.

Stamnes, K., Tsay, S.-C., Wiscombe, W., and Jayaweera, K.: Numerically stable algorithm for discrete-ordinate-method radiative transfer in multiple scattering and emitting layered media, Appl. Opt., 27, 2502, https://doi.org/10.1364/AO.27.002502, 1988.

Steinbrecht, W., Claude, H., Köhler, U., and Hoinka, K. P.: Correlations between tropopause height and total ozone: Implications for long-term changes, J. Geophys. Res. Atmospheres, 103, 19 183–19 192, https://doi.org/10.1029/98JD01929, 1998.

Svendby, T.: GUV total ozone column and effective cloud transmittance from three Norwegian sites 1995-2019 (Version v2.0), https://doi.org/10.5281/zenodo.4773478, 2021.

Svendby, T., Bernet, L., and Dahlback, A.: Brewer Global Iradiance (GI) total ozone data at two Norwegian sites (2000 to 2020) (version v1.0), https://doi.org/10.5281/zenodo.6760244, 2022.

Svendby, T. M. and Dahlback, A.: Statistical analysis of total ozone measurements in Oslo, Norway, 1978–1998, J. Geophys. Res., 109, 1–11, https://doi.org/10.1029/2004jd004679, 2004.

Svendby, T. M., Johnsen, B., Kylling, A., Dahlback, A., Bernhard, G., Hansen, G., Petkov, B., and Vitale, V.: GUV long-term measurements of total ozone column and effective cloud transmittance at three Norwegian sites, Atmospheric Chem. Phys., pp. 1–29, https://doi.org/10.5194/acp-21-7881-2021, 2021.

Thompson, A. M., Stauffer, R. M., Wargan, K., Witte, J. C., Kollonige, D. E., and Ziemke, J. R.: Regional and Seasonal Trends in Tropical Ozone From SHADOZ Profiles: Reference for Models and Satellite Products, JGR Atmospheres, 126, https://doi.org/10.1029/2021JD034691, 2021.

Tiao, G. C., Reinsel, G. C., Xu, D., Pedrick, J. H., Zhu, X., Miller, A. J., DeLuisi, J. J., Mateer, C. L., and Wuebbles, D. J.: Effects of autocorrelation and temporal sampling schemes, J. Geophys. Res., 95, 20 507–20 517, 1990.

Tung, K. K. and Yang, H.: Global QBO in Circulation and Ozone. Part I: Reexamination of Observational Evidence, J. Atmospheric Sci., 51, 2699–2707, https://doi.org/10.1175/1520-0469(1994)051<2699:GQICAO>2.0.CO;2, 1994.

USask ARG and LOTUS Group: LOTUS regression, https://arg.usask.ca/docs/LOTUS_regression/, 2017.

Van Malderen, R., De Muer, D., De Backer, H., Poyraz, D., Verstraeten, W. W., De Bock, V., Delcloo, A. W., Mangold, A., Laffineur, Q., Allaart, M., Fierens, F., and Thouret, V.: Fifty years of balloon-borne ozone profile measurements at Uccle, Belgium: A short history, the scientific relevance, and the achievements in understanding the vertical ozone distribution, Atmospheric Chem. Phys., 21, 12 385–12 411, https://doi.org/10.5194/acp-21-12385-2021, 2021.

Varotsos, C., Cartalis, C., Vlamakis, A., Tzanis, C., and Keramitsoglou, I.: The long-term coupling between column ozone and tropopause properties, J. Clim., 17, 3843–3854, https://doi.org/10.1175/1520-0442(2004)017<3843:TLCBCO>2.0.CO;2, 2004.

Veefkind, P.: OMI/Aura Ozone (O3) DOAS Total Column 1-Orbit L2 Swath 13x24 km V003, Goddard Earth Sciences Data and Information Services Center (GES DISC), Greenbelt, MD, USA, https://doi.org/10.5067/Aura/OMI/DATA2012, 2006.

Vigouroux, C., Blumenstock, T., Coffey, M., Errera, Q., Garciá, O., Jones, N. B., Hannigan, J. W., Hase, F., Liley, B., Mahieu, E., Mellqvist, J., Notholt, J., Palm, M., Persson, G., Schneider, M., Servais, C., Smale, D., Thölix, L., and De Mazière, M.: Trends of ozone total columns and vertical distribution from FTIR observations at eight NDACC stations around the globe, Atmospheric Chem. Phys., 15, 2915–2933, https://doi.org/10.5194/acp-15-2915-2015, 2015.

von der Gathen, P., Kivi, R., Wohltmann, I., Salawitch, R. J., and Rex, M.: Climate change favours large seasonal loss of Arctic ozone, Nat. Commun., 12, https://doi.org/10.1038/s41467-021-24089-6, 2021.

Wang, W., Hong, J., Shangguan, M., Wang, H., Jiang, W., and Zhao, S.: Zonally Asymmetric Influences of the Quasi-Biennial Oscillation on Stratospheric Ozone, Atmospheric Chem. Phys. Discuss., pp. 1–26, https://doi.org/10.5194/acp-2022-174, 2022.

Weber, M., Coldewey-Egbers, M., Fioletov, V. E., Frith, S. M., Wild, J. D., Burrows, J. P., Long, C. S., and Loyola, D.: Total ozone trends from 1979 to 2016 derived from five merged observational datasets – the emergence into ozone recovery, Atmospheric Chem. Phys., 18, 2097–2117, https://doi.org/10.5194/acp-18-2097-2018, 2018.

Weber, M., Arosio, C., Coldewey-Egbers, M., Fioletov, V. E., Frith, S. M., Wild, J. D., Tourpali, K., Burrows, J. P., and Loyola, D.: Global total ozone recovery trends attributed to ozone-depleting substance (ODS) changes derived from five merged ozone datasets, Atmos. Chem. Phys., 22, 6843–6859, https://doi.org/10.5194/acp-22-6843-2022, 2022.

WMO: Guide to meteorological instruments and methods of observation, WMO-NO. 8, World Meteorological Organization, Geneva, Switzerland, seventh edn., 2008.

WMO: Scientific Assessment of Ozone Depletion: 2018, p. 588, World Meteorological Organization, Global Ozone Research and Monitoring Project - Report No. 58, Geneva, Switzerland, 2018.

670   Wohltmann, I., Rex, M., Brunner, D., and Mäder, J.: Integrated equivalent latitude as a proxy for dynamical changes in ozone column, Geophys. Res. Lett., 32, 1–4, https://doi.org/10.1029/2005GL022497, 2005.

Zhang, J., Tian, W., Xie, F., Sang, W., Guo, D., Chipperfield, M., Feng, W., and Hu, D.: Zonally asymmetric trends of winter total column ozone in the northern middle latitudes, Clim Dyn, 52, 4483–4500, https://doi.org/10.1007/s00382-018-4393-y, 2019.